STUDY OF HEAT TRANSFER DURING PIERCING PROCESS OF OXYFUEL GAS CUTTING

N. Osawa, J. Sawamura, Y. Ikegami and N. Okamoto

ABSTRACT

The heat transfer parameters, the local heat transfer coefficient, α, and the gas temperature adjacent to the plate, T_G, are nearly unchanged with time during preheating for oxyfuel gas cutting. A genetic algorithm (GA)-based identification technique for α and T_G is proposed. The validity of the proposed technique and the accuracy of the identified parameters are examined by comparing the measured and calculated plate back face temperatures during spot heating tests. Hydrogen-LP mixed gas and LPG are used as preheating gases in these tests. It is considered that the plate temperatures during preheating for piercing can be calculated by using α and T_G identified in spot heating tests. The minimum piercing time is estimated by calculating the time until the plate heating face temperature reaches the kindling temperature. The validity of the above assumption is examined by comparing the estimated and measured minimum piercing times for hydrogen-LP mixed gas and LPG. As a result, the following are found: 1) The plate temperatures during spot heating tests calculated by using the identified heat input parameters agree well with the ones measured. This demonstrates the accuracy of the identified parameters and the validity of the proposed heat transfer simulation technique. 2) The heat flux of a hydrogen-LP mixed gas flame around the preheating gas ejection hole is 40 % greater than that of a LPG flame, while the total calorific value of hydrogen-LP mixed gas is 25 % lower than that of LPG. This result shows that it is not appropriate to evaluate the thermal effect of the preheat flame only from the total calorific value alone. 3) The calculated time for the plate face temperature to exceed the steel's kindling temperature almost agrees with the minimum piercing time observed in piercing tests. For the first time, it is possible to anticipate the piercing time by numerical simulation.

IIW-Thesaurus keywords: Computation; Flame cutting; Heat flow; Hydrogen; Liquefied gases; Mixtures; Preheating.

1 Introduction

Thermal cutting is widely used in the manufacture of heavy equipment and in the construction of structural members for steel structures. In recent years, the demand for heavy thick steel plates with over 50 mm thickness has increased as upsizing of ships, offshore structures and buildings. Oxyfuel gas cutting is the only cutting method for such thick plates. Oxyfuel gas cutting has been gaining renewed attention.

The function of the preheating flame in oxyfuel gas cutting was studied by Suitsu and Yasuda [1, 2] and Nakanishi [3-5], but the relation between the preheating flame conditions (fuel gas, gas conditions, the total calorific value, etc.) and the cutting performances (cutting speed, kerf quality, thermal distortion, etc.) has not yet been fully clarified. On account of this, the adjustment of the preheating flame has not been done by automation, but by skilled workers. In current times, the shortage of skilled workers has become critical, and the desire is strong to automate this process.

In recent years, there has been a move towards using oxy-hydrogen cutting in industries. The use of hydrogen can reduce the emission of greenhouse gases. It is reported that hydrogen preheating reduces the thermal distortion of workpieces and allows for improvement in cutting performance. The precise mechanism of these improvements has not yet been clarified, and it is difficult to optimize the hydrogen preheating flame. For this reason, oxy-hydrogen cutting has not become widespread.

It is expected that the preheating flame adjustment can be automated. The optimization of the oxy-hydrogen cutting condition thus becomes easier if the relation between the preheating flame conditions and the cutting performance is clarified. This can be achieved by closely examining the relation between the flame conditions and the thermal effect. It is difficult to examine the thermal effect during oxyfuel gas cutting because both the heat transfer between the gas flame and the workpiece and the exothermic reaction between the oxygen and the iron arise. The study of the thermal effects in piercing processes is a good way to get things started.

Doc. IIW-2152, recommended for publication by Commission I "Thermal Cutting and Surfacing."

There are some studies on the thermal effect of preheating in piercing processes (e.g., Sato *et al.* [6]), but they failed to give a simple explanation on the relation between the heat input and the piercing performance. In most of these studies, the heat input was estimated from the total calorific value of the fuel gas, and the heat flux was not examined directly. It is considered that the direct heat flux estimation is needed to clarify the heat effect. Terasaki *et al.* [7] examined the heat flux in the oxyfuel gas cutting process quantitatively by using the heat flux determination technique proposed by Tsuji and Okumura [8]. In this flux determination technique, the heat flux distribution around the torch is assumed to remain unchanged with time. This approximation is not valid for spot heating cases in which the workpiece temperature rises remarkably. Terasaki's results cannot be utilized in the study of piercing processes.

The authors (Osawa *et al.* [9]) developed a genetic algorithm (GA)-based heat transfer estimation technique which can be applied to cases where the heating face temperature exceeds the steel's kindling temperature. The relation between the flame condition and the heat transfer can be examined with a high degree of precision by using this technique. In their study, the genetic representation of heat transfer parameters was developed for line heating analyses. It is necessary to modify the genetic representation so that it can represent the features of the preheating flame in oxyfuel gas cutting.

In this study, the author's GA-based heat transfer estimation technique is modified so that it can be applied to the analyses of preheating processes. The validity of the proposed technique and the accuracy of the identified parameters are examined by comparing the measured and calculated plate temperatures during spot heating tests. H_2/LP gas (combining propane gas with hydrogen and oxygen generated through water electrolysis) and LPG are used as preheating gases. The plate temperature during the piercing process is calculated using these identified parameters, and the piercing performance is estimated by calculating the time until the plate face temperature reaches the kindling temperature. The validity of the proposed piercing performance estimation method is examined by comparing the estimated and measured minimum piercing times.

2 Theory

2.1 Parameters for heat transfer between gas flame and steel plate

The authors (Tomita *et al.* [10]) measured the transient gas temperature field within the combustion flame during spot heating tests with the laser-induced fluorescence (LIF) measurement system. They found that the thermal-flow field of the heating gas becomes stable in an extremely short time and remains unchanged during spot heating. This means that the temperature of the gas adjacent to the plate T_G and the local heat transfer coefficient α can be considered to remain nearly unchanged with time. This leads to a linear relationship between flux q and heating face temperature T_S.

Time histories of plate back surface temperature T_B are measured during a spot heating test. Time histories of flux and heating face temperature, q and T_S, can be estimated by inverse heat conduction (IHC) analysis from the measured T_B. T_G and α can be identified by a linear regression analysis of the relation between q and T_S. The authors (Osawa *et al.* [11-13]) proposed an IHC technique for the estimation of q and T_S. However, they sometimes failed to estimate them because the IHC problem is extremely sensitive to measurement errors. This problem can be overcome by estimating time-independent T_G and α directly.

In such analyses, the gradient-based search techniques are not optimum because they can be trapped in local minima and require the objective function and its derivatives to be continuous within the search space. Stochastic optimization techniques, such as genetic algorithms (GA), can overcome these problems and they can find the global solution. The reader is referred to Chakraborti [14] for a review of how GA is utilized in material processing. The authors (Osawa *et al.* [9]) proposed a GA-based direct identification technique for T_G and α. The validity of this technique was demonstrated by comparing the identified T_G and the one measured with the LIF system.

2.2 Genetic representation of heat transfer parameters

Hereafter, r denotes the distance from the nozzle centre, and r_0, r_E the distances from the nozzle centre to the spouts of preheating gas and the outer end of the analysis region. The region with $0 < r < r_0$ is called 'inner region', and that with $r_0 < r < r_E$ 'outer region'. In the GA analysis of Osawa *et al.* [9], the genetic representations were formulated so that T_G and α show their maximums at $r = 0$. These representations cannot be used for oxyfuel gas cutting nozzles because T_G and α must show their maximum at $r = r_0$. We can assume the following in the analyses of preheating for oxyfuel gas cutting:

i) T_G shows its maximum at $r = r_0$, and the maximum T_G is close to the theoretical flame temperature. T_G approaches room temperature at $r = \infty$;

ii) α shows its maximum at $r = r_0$. α approaches the natural convection heat transfer coefficient when $r = \infty$. Based on these assumptions, T_G and α are represented as follows in this study:

a. Set the upper and lower bounds of T_G and α at $r = 0$, r_0 and r_E:

$$T_{C,\min}, T_{C,\max}, T_{0,\min}, T_{0,\max}, T_{E,\min}, T_{E,\max}, \alpha_{C,\min}, \alpha_{C,\max}, \alpha_{0,\min}, \alpha_{0,\max}, \alpha_{E,\min}, \alpha_{E,\max}$$

b. Give T_G and α at $r = 0$, $r = r_0$ and $r = r_E$ as:

$$\left.\begin{aligned} T_C &= T_{C,\min} + d_C\left(T_{C,\max} - T_{C,\min}\right) \\ \alpha_C &= \alpha_{C,\min} + e_C\left(\alpha_{C,\max} - \alpha_{C,\min}\right) \\ T_0 &= T_{0,\min} + d_0\left(T_{0,\max} - T_{0,\min}\right) \\ \alpha_0 &= \alpha_{0,\min} + e_0\left(\alpha_{0,\max} - \alpha_{0,\min}\right) \\ T_E &= T_{E,\min} + d_E\left(T_{E,\max} - T_{E,\min}\right) \\ \alpha_E &= \alpha_{E,\min} + e_E\left(\alpha_{E,\max} - \alpha_{E,\min}\right) \end{aligned}\right\} \quad (1)$$

where

$d_C, d_0, d_E, e_C, e_0, e_E$ are real numbers ranging from 0 to 1.

c. Arrange n_I number of control points (CP) in 'inner region', and enumerate them as $i_I = 1,2,\ldots,n_I$ in order of the increasing distance from the spout ($r = r_0$). Give T_G and α at each CP as:

$$\left.\begin{aligned} T_{I1} &= T_C + f_1\left(T_{\max} - T_C\right),\ \alpha_{I1} = \alpha_C + g_1\left(\alpha_{\max} - \alpha_C\right) \\ T_{I2} &= T_C + f_2\left(T_{I1} - T_C\right),\ \alpha_{I2} = \alpha_C + g_2\left(\alpha_{I1} - \alpha_C\right) \\ &\vdots \end{aligned}\right\} \quad (2)$$

where

$f_1, g_1, f_2, g_2, \ldots$ are real numbers ranging from 0 to 1.

d. In the same manner as (c), arrange n_O number of CPs in 'outer region', and enumerate them as $i_O = 1,2,\ldots,n_O$ in order of the increasing distance from the spout ($r = r_0$). Give T_G and α at each CP as:

$$\left.\begin{aligned} T_{O1} &= T_E + h_{O1}\left(T_{\max} - T_E\right),\ \alpha_{O1} = \alpha_E + k_{O1}\left(\alpha_{\max} - \alpha_E\right) \\ T_{O2} &= T_E + h_{O2}\left(T_{O1} - T_E\right),\ \alpha_{O2} = \alpha_E + k_{O2}\left(\alpha_{O1} - \alpha_E\right) \\ &\vdots \end{aligned}\right\} \quad (3)$$

where

$h_1, k_1, h_2, k_2, \ldots$ are real numbers ranging from 0 to 1.

e. T_G and α between CPs are given by linear or 3rd order spline interpolation.

$2 \times 3 + 2 \times n_I + 2 \times n_O$ number of real numbers

$d_C, d_0, d_E, e_C, e_0, e_E, f_1, g_1, f_2, g_2, \ldots, h_1, k_1, h_2, k_2, \ldots$ are the genes of GA analysis. An example of genetic representation of T_G and α is shown in Figure 1.

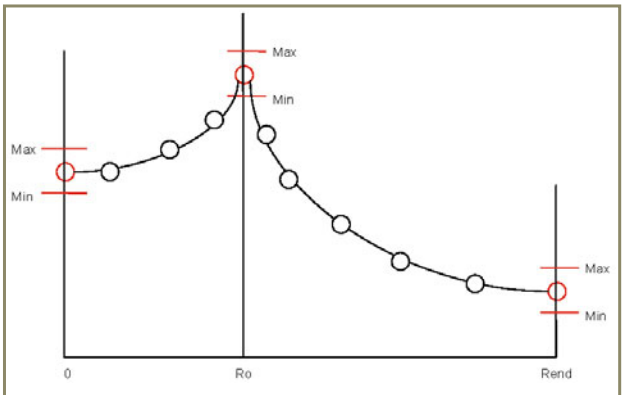

Figure 1 – Genetic representation of the distribution of heat transient parameters

2.3 Fitness function

The distributions of T_G and α are identified by carrying out spot heating tests of thin circular steel plates. Let $B_{J,K}$ be the measured plate back face temperature at the J-th measurement point ($J = 1,2,\ldots,N_B$) at time t_K ($K = 1,2,\ldots,N_T$), and $Y_{J,K}$ be the calculated temperature at the same point and same time. The fitness function E is defined as:

$$E = \frac{\sum_{K=1}^{N_T}\sum_{J=1}^{N_B}\left(Y_{J,K} - B_{J,K}\right)^2}{\sum_{K=1}^{N_T}\sum_{J=1}^{N_B}\left(B_{J,K}\right)^2} \quad (4)$$

E in Equation (4) approaches zero when the calculated back face temperatures agree well with the measured ones. The genes, $d_C, d_0, d_E, e_C, e_0, e_E, f_1, g_1, f_2, g_2, \ldots, h_1, k_1, h_2, k_2, \ldots$ are optimized by GA analysis so that E is minimized.

3 Identification of the heat transfer parameters

3.1 Spot heating tests

A circular mild steel disk of diameter d = 300 mm and 6 mm thickness, shown in Figure 2, is arranged horizontally and a preheating nozzle is positioned above the disk. The back surface of the disk is coated with a heat insulating material, and the centre of the plate is heated by H_2/LP gas (52 % H_2-22 % C_3H_8-26 % O_2) and LPG flame. The Koike Sanso Kogyo type 6023 gas cutting torch was used, and the Koike Sanso Kogyo types 105A-2 (for H_2/LP gas) and 106-2 (for LPG) were used for gas nozzles. These nozzles are suitable for the cutting of steel plates with thicknesses ranging from 15 mm to 30 mm. The spout geometries of the nozzles are shown in Figure 3. The distances from the nozzle centre to the preheating gas spouts, r_0, is 3.0 mm for both nozzles. The thickness of the test specimen (6 mm) is much smaller than the recommended thickness (> 15 mm), because it is necessary to increase the responsiveness of the back face tempera-

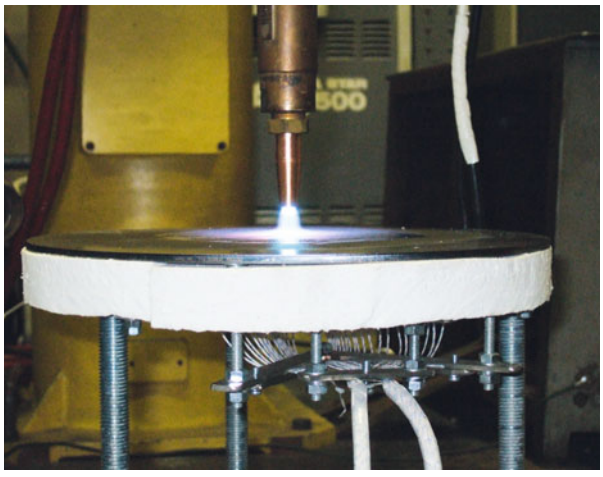

Figure 2 – Test specimen used in spot heating tests

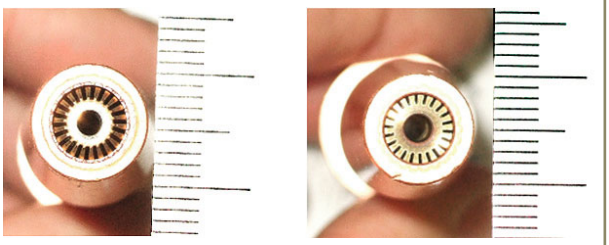

a) H_2/LP gas b) LPG

Figure 3 – Preheating gas nozzles for H_2/LP gas and LPG

ture to the heat flux enough to eliminate the problem of bad positioning of the IHC.

The pressure and flow of the fuel gas and oxygen are shown in Table 1. The gas conditions for LPG were chosen by following the manufacturer's recommendation for groove cutting. Those for H_2/LP gas are optimized by the authors after trial and error. The flow of oxygen was determined so that a natural flame was obtained. The oxygen flow for LPG is about 76 % of that required to achieve the theoretical mixture ratio, and that for H_2/LP gas is about 79 % of that required.

The white corn length of the gas flame was about 5 mm for both gases. The distance between the workpiece and the nozzle was 6 mm. The pressure and flow were controlled by mass-flow rate sensors Yamatake CMS500 (for H_2/LP gas), CMQ200 (for LPG), CMS50 (for preheating oxygen) and CMS500 (for cutting oxygen). The total calorific values of each gas are also presented in Table 1. The calorific value of LPG is calculated by assuming that the calorific value of LPG and C_3H_8 are 92.6 MJ/h. That of H_2/LP gas is calculated by assuming that the calorific value of hydrogen is 5.34 MJ/h. Table 1 shows that the total calorific value of H_2/LP gas is about 75 % of that of LPG.

The time histories of the plate back face temperature were measured by K-type thermoelectric couples (TCs) with a sheath diameter of 0.1 mm welded on the plate back surface. The outputs of thermocouples were

Table 1 – Heating conditions employed in spot heating tests

	H_2/LP gas	LPG
Distance between nozzle and plate [mm]	6.0	6.0
Pressure of burning gas [MPa]	0.038	0.023
Flow of burning gas [l/min]	16.0[a)]	6.0
Pressure of oxygen [MPa]	0.053	0.077
Flow of oxygen [l/min]	13.0[b)]	22.8
Total calorific value [MJ/h]	24.9[c)]	33.3

[a)] H_2: 8.32 l/min, LP: 3.52 l/min, O_2: 4.16 l/min
[b)] O_2 of 4.16 l/min is supplied additionally from the fuel gas.
[c)] H_2: 5.34 MJ/h., LP: 19.5MJ/h.

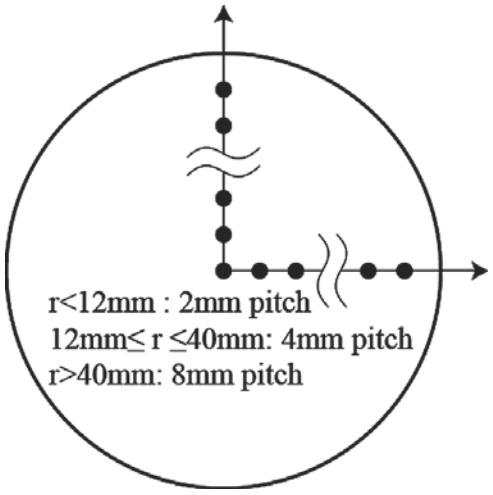

Figure 4 – Arrangement of thermocouples for spot heating tests

recorded on a personal computer every 1.0 s. As shown in Figure 4, TCs were arranged in a radial direction from the centre to a point 104 mm away from the centre. The intervals of the points are 2 mm for $r \leq 12$ mm, 4 mm for 12 mm $< r \leq 40$ mm and 8 mm for $r > 40$ mm. For $r > 0$, the average of two measurements for the same r is taken as the representative value. In the tests, heating ceased within about 5 s. The gas torch was controlled by a welding robot FANUC ARC Mate DR-4000.

3.2 Optimization analysis

$Y_{J,K}$ in Equation (4) is calculated by carrying out axisymmetric finite element (FE) direct heat conduction (DHC) analyses in which $T_G(r)$ and $\alpha(r)$, represented by Equations (1), (2) and (3), are applied as boundary conditions.

The temperature dependencies of the material properties shown in Figure 5 are used. DHC analysis is performed by using an in-house axisymmetric thermal FE code. The

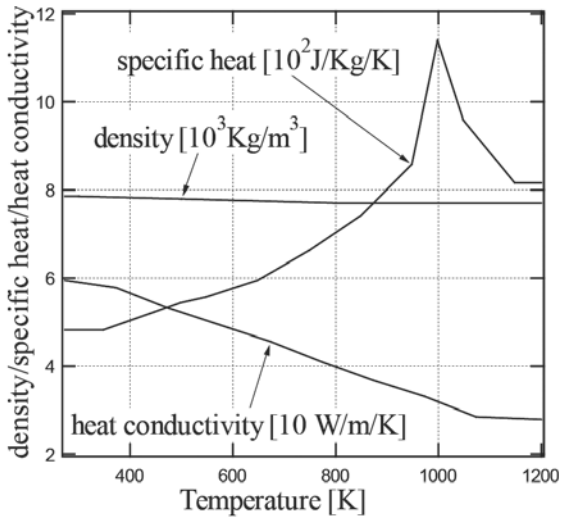

Figure 5 – Temperature dependency of the material properties

Figure 6 – The FE mesh used in direct heat conduction analysis of spot heating tests

Table 2 – Model dimensions of the FE mesh for DHC analysis of the spot heating tests

Model dimensions [m]	0.3 × 0.006
Num. of elements	40 × 40 × 6
Max./Min. element size in x dir [× 10^{-3} m]	3.44 / 13.8
Max./Min. element size in y dir [× 10^{-3} m]	3.44 / 13.8
Max./Min. element size in z dir [× 10^{-4} m]	5.04 / 16.8

FE mesh and its dimensions are shown in Figure 6 and Table 2. The FE model comprises 4 node isoparametric quadrilateral elements, and the back surface is assumed to be adiabatic. The initial temperature is 300 K. The convective heat transfer between plate and air is evaluated at the outer end, and its coefficient is 480 W/(m^{2}K). In time integration, iterative calculation by Newman's method is repeated until the residual temperature norm becomes less than 10^{-6} times as much as the nodal temperature norm. The numerical damping is 0.01, and the time increment ranges from 10^{-4} to 5 × 10^{-2} s.

The GA analyses are carried out by using the commercial optimization software, Optimus 5.2 (Noesis Solutions [15]). The genes $d_C, d_0, d_E, e_C, e_0, e_E, f_1, g_1, f_2, g_2, \ldots, h_1, k_1, h_2, k_2, \ldots$ are optimized so that E in Equation (4) is minimized by Self-Adaptive-Evolution algorithm (Schwefel, [16]).

Table 3 shows the upper and lower bounds of T_G and α at $r = 0$, r_0 and r_E. CPs are arranged at r = 1.2, 1.6, 1.8 mm for 'inner region', and at r = 4.28, 7.32, 13.4, 21.0, 32.4 mm for 'outer region'. T_G and α between CPs are estimated by linear interpolation because the difference in the calculated back face temperatures derived from spline interpolation and that from linear interpolation is negligible. The control parameters of self-adaptive evolution are shown in Table 4.

Table 3 – The upper and lower bounds of T_G and α at $r = 0$, r_0 and r_E

r	Heat transfer coefficient α [W/(m^{2}K)]		Gas temperature right on the plate T_G [K]	
	min.	max.	min.	max.
0	1 900	2 600	3 400	3 700
r_0	2 500	3 500	3 800	4 200
r_E	480	600	867	1 500

Table 4 – Control parameters of self-adaptive evolution employed in the analyses

Random seed	1
Number of parents	5
Sexuality	5
Population size	60
Initial step width	1
Average stopping stepwidth	0.01
Stepwidth mutation factor	1.3
Max. number of iterations	30

3.3 The heat transfer parameters: results

The identified T_G and α for H_2/LP gas and LPG are shown in Figure 7. $Y_{J,K}$ in Equation (4) can be calculated by DHC analysis using these parameters as the thermal boundary conditions. The accuracy of the identified parameters can be examined by comparing $Y_{J,K}$ with $B_{J,K}$. The DHC analysis is performed by the FE code used in the GA analyses. The material properties shown in Figure 5 and FE mesh shown in Figure 6 are employed, and the calculation conditions are the same as those for IHC analysis. Figure 8 compares the measured and calculated back surface temperatures which coincide well. These results demonstrate the accuracy of the identified parameters and the validity of the hypotheses on heat transfer between flame and plate.

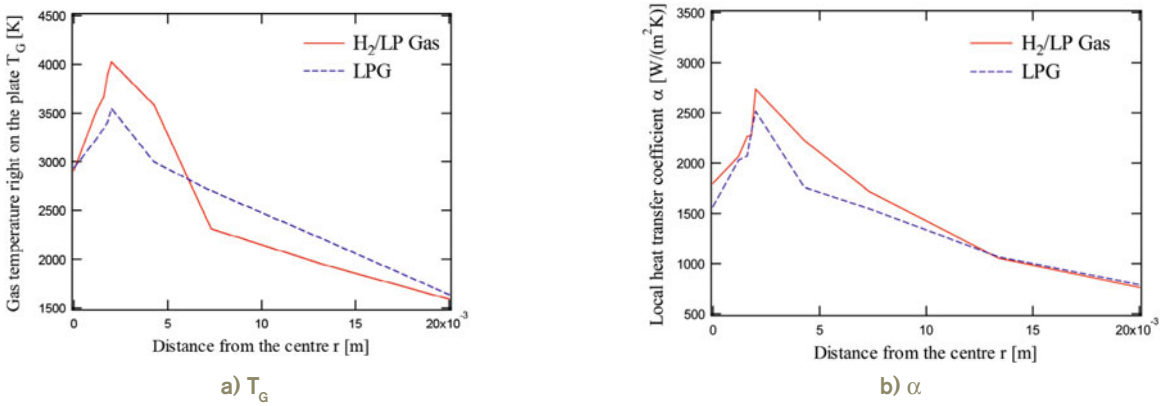

a) T_G b) α

Figure 7 – Distribution of gas temperatures right on the plate T_G and α during spot heating tests

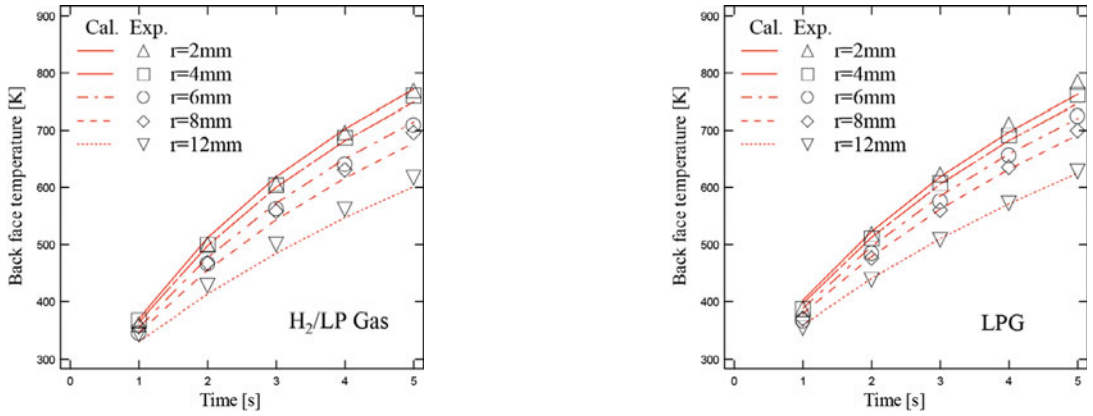

Figure 8 – Comparison of the measured plate back surface temperatures during spot heating tests with those obtained by direct heat conduction analysis using the identified T_G and α of H_2/LP gas and LPG

3.4 The heat flux during spot heating

Figure 9 shows the calculated heat flux distribution q(t;r) at time t = 0.5, 2.5 and 4.5 s for H_2/LP gas and LPG. These figures show that q decreases with time. q is the highest at $r = r_0$ for both H_2/LP and LPG. q just below the spout ($r = r_0$) of H_2/LP gas is about 40 % higher than that of LPG. This means that the heat transfer of H_2/LP gas is greater than that of LPG, even though the total calorific value of H_2/LP gas is lower than LPG, as shown in Table 1.

Figure 10 shows the change of the ratios of T_G and α of H_2/LP gas to those of LPG with respect to r. This figure shows that these ratios show their maximum (about 145 % for T_G and α) at r = 4.5 mm, and the ratio of α is maintained at a high level (> 100 %) within $r \leq 10$ mm, while the ratio of T_G decreases with r rapidly and the magnitude relation is reversed when r > 6 mm. In short, the high T_G region of H_2/LP gas is smaller than that of LPG, and α of H_2/LP gas is greater than that of LPG.

It is considered that the superiority of H_2/LP gas in α is the main cause of the negative correlation between the total calorific value and the heat flux. The burning velocity of hydrogen is about 3.4 times higher than LPG. This results in the flow rate of H_2/LP gas being about 2.5 times higher than that of LPG. It is assumed that this difference makes the impinging jet heat transfer of H_2/LP gas greater than that of LPG. The results described above show that it is not appropriate to evaluate the thermal effect of preheating only from the total calorific value.

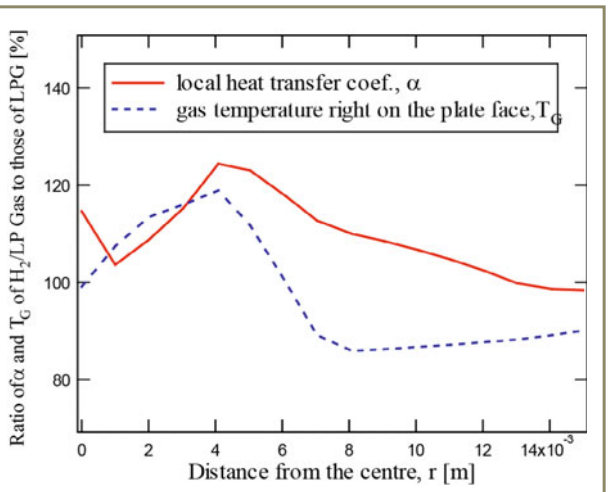

Figure 10 – Ratio of α and T_G of H_2/LP gas to those of LPG

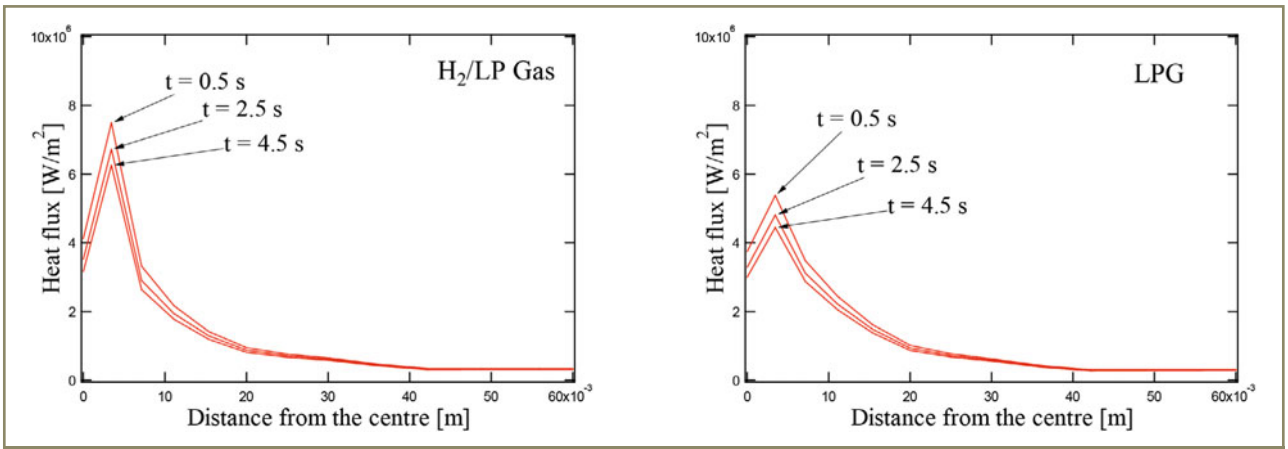

Figure 9 – Heat flux distribution during the spot heating test with H_2/LP gas and LPG

4 Estimation of piercing performances

4.1 Piercing tests

Rectangular steel plates of 200 mm length, 200 mm width and 12 mm thickness, shown in Figure 11, were heated by H_2/LP gas and LPG preheating gas flame. The cutting torch was located at a point 50 mm away from the two edges of the plate. The piercing conditions (nozzle, gas conditions and nozzle height) are the same as those shown in Table 1. The thickness (12 mm) is comparable with the recommended thickness of cutting nozzles (15 mm to 30 mm).

The nozzle height was kept at 6 mm during preheating. When the preheating was finished, the torch was moved 10 mm upward and the supply of cutting oxygen was started. The flow rate and pressure of the cutting oxygen was 150 l/min and 0.3 MPa. The 'minimum piercing time' was measured by gradually extending the preheating time by 5 s per trial until the plate was successfully pierced. The temperature distribution on the plate heating face was measured by an infrared camera, FLIR SYSTEM SC620NTSC, from about 1.5 m away. The radiation factor 0.97 was used in the temperature measurements. The width of the temperature measurement region was about 300 mm, and the video resolution was 640 × 480.

The measured 'minimum piercing time' was 20 s for H_2/LP gas and 30 s for LPG. It was observed that the diameter of the area in which the temperature exceeded the steel's kindling temperature (about 1 300 K) after preheating was larger than 10 mm for the cases where the plate was successfully pierced.

4.2 Plate temperature estimation during piercing tests

The authors (Osawa *et al.* [13]) showed that the plate temperature can be estimated accurately by assuming

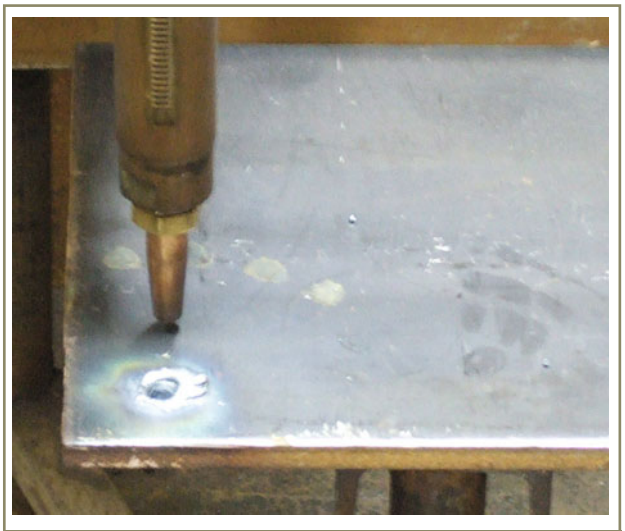

Figure 11 – Test specimen used in piercing tests

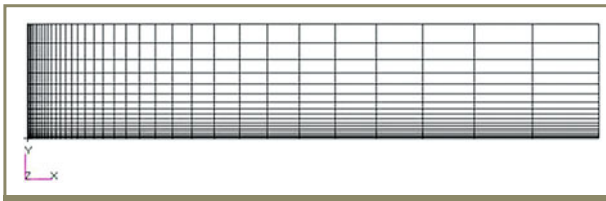

Figure 12 – The FE mesh used in direct heat conduction analysis of piercing tests

that the T_G and α remain unchanged, even if the heating face temperature exceeds 1 000 K. This leads us to expect the possibility of estimating the time until the plate face temperature exceeds the steel's kindling temperature in the piercing tests by using T_G and α identified in the spot heating tests.

The plate temperature during the preheating process is calculated by using the FE code used in the GA analyses. The material properties shown in Figure 5 and FE mesh shown in Figure 12 are employed. The material properties and calculation conditions are the same as those for IHC analysis. This FE model is an axisymmetric model of a circular plate with a radius of 60 mm, and it comprises 4 node isoparametric quadrilateral elements. The element edge length ranges from 0.1 mm to 6.95 mm in radial direction, and from 0.1 mm to 2.02 mm in through-thickness direction.

Figure 13 shows the calculated plate heating face temperatures at r = 0, 3 mm and 6 mm during piercing tests preheated by H_2/LP gas and LPG. The abscissa of this figure is the elapsed time from the beginning of the preheating process, t. Let t_{wpk} (warm-up period for kindling) be the time until the heating face temperature at r = 6 mm exceeds the steel's kindling temperature (1 300 K). It is shown that t_{wpk} is 22.5 s for H_2/LP gas and 28.8 s for LPG.

The results of the infrared camera measurements lead us to an assumption that the prerequisite for the success of piercing is the generation of a plate surface area with a diameter larger than 10 mm, within which the heating face temperature exceeds 1 300 K. Therefore, it can be

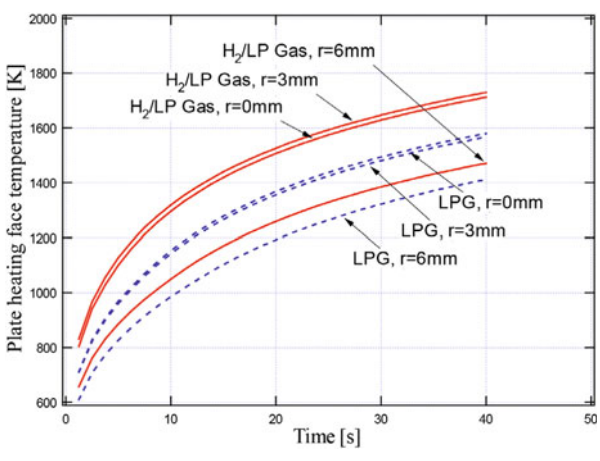

Figure 13 – Time histories of the plate heating face during piercing tests

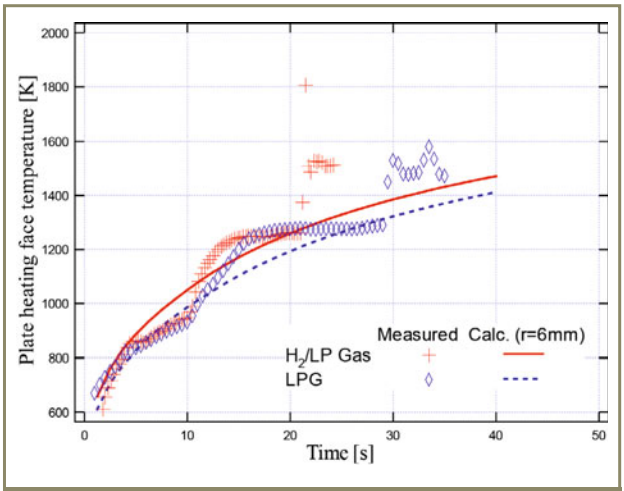

Figure 14 – Comparison of measured and calculated plate heating face temperatures during piercing tests

considered that t_{wpk} is approximately equal to the minimum piercing time. The calculated values of t_{wpk} (H_2/LP gas: 22.5 s, LPG: 28.8 s) almost agree with the measured minimum piercing times (H_2/LP gas: 20 s, LPG: 30 s).

Figure 14 shows the measured plate heating face temperatures for tests with H_2/LP gas and LPG. They are the average temperatures in the region just below the nozzle with a diameter of about 10 mm, and it is considered that these measured temperatures correspond to the calculated temperature at r = 6 mm. Calculated heating face temperatures at r = 6 mm are also plotted in this figure. Measured temperatures jump sharply in response to the beginning of the supply of cutting oxygen (at t = 20 s for H_2/LP gas and t = 30 s for LPG). Measured data show fluctuations occurring at about a 5 s-rate of temperature increase. It is supposed that these fluctuations are caused by changes in plate surface condition. Figure 14 shows that the calculated temperatures almost agree with the measured ones when we remove this low-frequency noise.

From the results described above, we can conclude that the plate temperature during the piercing preheating process can be calculated with a high degree of accuracy by using T_G and α identified in the spot heating tests. For the first time, it is possible to anticipate the piercing time by numerical simulation.

Figures 15 a) and b) show the temperature distributions on the cross-section of the plate at the end of the preheating process (H_2/LP gas: 20 s, LPG: 30 s). These figures are illustrated upside down, and the lower surface is the heating face. The temperature distributions on the heating face of H_2/LP gas and LPG are generally similar, while the cross-sectional temperature distributions are quite different. The region in which the temperature exceeds the mechanical melting point (1 000 K) reaches the back face for LPG, while its border is at the mid-point of the cross-section. This shows that the volume of inherent strain generation region (that is, the degree of the thermal distortion) is not positively correlated with the magnitude of the heat flux.

5 Conclusions

The heat transfer parameters, the local heat transfer coefficient, α, and the gas temperature adjacent to the plate, T_G, are nearly unchanged with time during preheating for oxyfuel gas cutting. A genetic algorithm (GA)-based identification technique for α and T_G is proposed. The validity of the proposed technique and the accuracy of the identified parameters are examined by comparing the measured and calculated plate back face temperatures during spot heating tests. Hydrogen-LP mixed gas and LPG are used as preheating gases in these tests. It is considered that the plate temperatures during preheating for piercing can be calculated by using α and T_G identified in spot heating tests. The minimum piercing time is estimated by calculating the time until the plate heating face temperature reaches the kindling temperature. The validity of the above assumption is examined by comparing the estimated and measured minimum piercing times for hydrogen-LP mixed gas and LPG. As a result, the following are found:

1. The plate temperatures during spot heating tests calculated by using the identified heat input parameters agree well with those measured. This demonstrates the accuracy of the identified parameters and the validity of the proposed heat transfer simulation technique.
2. The heat flux of a hydrogen-LP mixed gas flame around the preheating gas ejection hole is 40 % larger

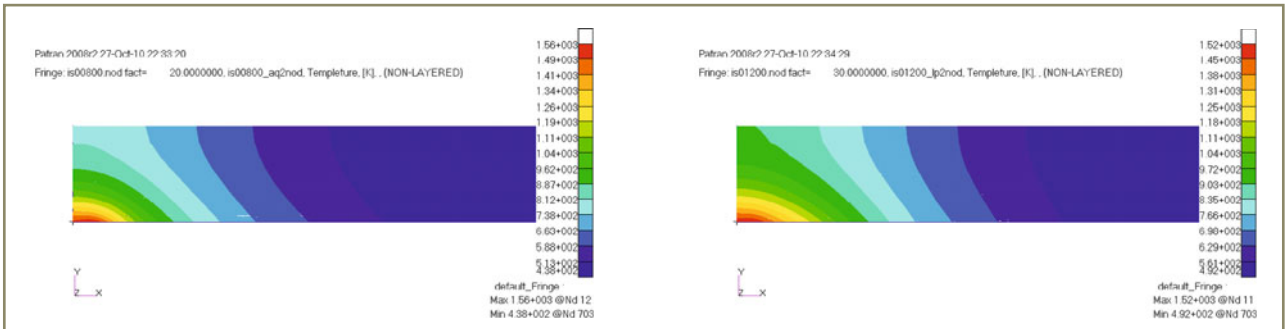

a) H_2/LP gas, time = 20 s

b) LPG, time = 30 s

Figure 15 – Plate temperature distributions at the times when the plate heating face temperature within a radius of 6 mm from the torch centre exceeds the burning temperature of steel (about 1 300 K)

than that of a LPG flame, while the total calorific value of hydrogen-LP mixed gas is 25 % lower than that of LPG. This result shows that it is not appropriate to evaluate the thermal effect of the preheat flame only from the total calorific value alone.

3. The calculated time until the plate face temperature exceeds the steel's kindling temperature almost agrees with the minimum piercing time observed in piercing tests. For the first time, it is possible to anticipate the piercing time by numerical simulation.
4. The minimum piercing time of a hydrogen-LP mixed gas flame is about 2/3 that of a LPG flame while the total calorific value of hydrogen-LP mixed gas is 25 % smaller than that of LPG. This result shows that it is not appropriate to evaluate the piercing performance only from the total calorific value alone.

Acknowledgements

This research was partially supported by the Ministry of Education, Science, Sports and Culture of Japan, Grant-in-Aid for Scientific Research (B), 2009-2011, 21360428. The cutting experiments were carried out at the R&D centre of Air Water Inc. The authors would like to acknowledge Mr Ryuji Yokoyama (Air Water Inc.) and Mr Ryohei Sugimoto (Graduate students, Osaka University) for their help with the experiments and analyses.

References

[1] Suitsu K. and Yasuda T.: Some investigations regarding oxygen cutting (Report 2) – Effect of steel temperature on the cutting efficiency, Journal of the Japan Welding Society, 1960, vol. 29, no. 6, pp. 490-497 (in Japanese).

[2] Suitsu K. and Yasuda T.: Some investigations regarding oxygen cutting (Report 5) – Effect of preheat variation on the cutting efficiency, Journal of the Japan Welding Society, 1961, vol. 30, no. 10, pp. 733-739 (in Japanese).

[3] Nakanishi M.: Study of preheating flame on oxygen cutting (Report 1) – Examination of the heating effect on the cut material, Journal of the Japan Welding Society, 1968, vol. 37, no. 8, pp. 839-844, (in Japanese).

[4] Nakanishi M.: Study of preheating flame on oxygen cutting (Report 2) – Activation effect on the material surface, Journal of the Japan Welding Society, 1968, vol. 37, no. 10, pp. 1108-1114 (in Japanese).

[5] Nakanishi M.: Study of preheating flame on oxygen cutting (Report 3) – Effect of preheating flame on material thickness to be cut, Journal of the Japan Welding Society, 1968, vol. 37, no. 11, pp. 1260-1287 (in Japanese).

[6] Sato T., Yamamoto Y., Kato T., Takeda T., Nagahori M. and Kamikihara H.: Influence of gas contents on characteristics of hydrogen-propane flame in oxyfuel gas cutting, Preprints of the National Meeting of JWS, 2008, vol. 83, pp. 78-79 (in Japanese).

[7] Terasaki T., Kitamura T. and Miyamoto M.: Heat input generated in plate by gas cutting process, Journal of the Japan Society of Naval Architects and Ocean Engineers, 2009, vol. 10, pp. 197-204 (in Japanese).

[8] Tsuji I. and Okumura Y.: A study on line heating process for plate bending of ship steels, Trans. The West-Japan Soc. Naval Architects, 1977, vol. 76, pp.149-160 (in Japanese).

[9] Osawa N., Hashimoto K., Sawamura J. and Tanaka H.: GA-based heat input estimation technique for simulation of shell forming by line-heating, Proceedings 18th International Offshore and Polar Engineering Conference, 2008, pp. 285-290.

[10] Tomita Y., Osawa N., Hashimoto K., Shinkai N., Sawamura J. and Matsuoka K.: Study on heat transfer between gas flame and plate during line-heating process, In: Y.S. Wu, W.C. Cui and G.J. Zhou (ed) Practical Design of Ships and Other Floating Structures, Elsevier, 2001, pp. 389-396.

[11] Osawa N., Tomita Y., Hashimoto K., Matsuoka K. and Kikuchi K.: Development of heat input estimation technique for line-heating process based on inverse heat conduction analysis, Proc. ISOPE2004, 2004, IV, pp. 133-140.

[12] Osawa N., Tomita Y., Hashimoto K. and Kikuchi J.: Improvement of the accuracy of heat input estimation during line heating process by using regularization method, Proc. the 9th Symposium on Practical Design of Ships and Offshore Floating Structures, 2004, pp. 974-981.

[13] Osawa N., Hashimoto K., Sawamura J., Kikuchi J., Deguchi Y. and Yamaura T.: Development of heat input estimation for simulation of shell forming by line-heating, Computer Modeling in Engineering & Sciences, 2007, vol. 20, no. 1, pp. 43-53.

[14] Chakraborti N.: Genetic algorithms in materials design and processing, International Materials Review 2004, vol. 49, no. 3–4, pp. 246–260.

[15] Noesis Solutions: OPTIMUS 5.2 – Users Manual, 2006.

[16] Schwefel H.P.: Numerical optimization of computer models, 1981, John Wiley & Sons, Chicester, New York.

About the authors

Prof. Naoki OSAWA (osawa@naoe.eng.osaka-u.ac.jp) and Prof. Junji SAWAMURA (sawamura@naoe.eng.osaka-u.ac.jp) are with Osaka University, Suita, Osaka, Japan. Mr Yuichi IKEGAMI (ikegamiy@Awi.co.jp) is with Air Water Inc., Wakayama, Japan. Mr Naoya OKAMOTO (Naoya_Okamoto@naoe.eng.osaka-u.ac.jp) is a graduate student of Graduate School of Engineering, Osaka University, Suita, Osaka, Japan.